Effects of Fe(II) and Hydrogen Peroxide Interaction upon Dissolving UO 2 under Geologic Repository Conditions

ARTICLE *in* ENVIRONMENTAL SCIENCE AND TECHNOLOGY · FEBRUARY 2005

Impact Factor: 5.33 · DOI: 10.1021/es040034x · Source: PubMed

6 AUTHORS, INCLUDING:

Maria Betti
European Commission
100 PUBLICATIONS **1,721** CITATIONS

SEE PROFILE

Environ. Sci. Technol. **2005**, *39,* 221−229

Effects of Fe(II) and Hydrogen Peroxide Interaction upon Dissolving UO_2 under Geologic Repository Conditions

M. AMME,*,† W. BORS,‡ C. MICHEL,‡ K. STETTMAIER,‡ G. RASMUSSEN,† AND M. BETTI†

European Commission, Joint Research Centre, Institute for Transuranium Elements, Postfach 2340, 76125 Karlsruhe, Germany, and Institute for Radiation Biology, GSF National Research Centre, Ingolstädter Landstrasse 1, 85764 Neuherberg, Germany

Iron redox cycling is supposed to be one of the major mechanisms that control the geochemical boundary conditions in the near field of a geologic repository for UO_2 spent nuclear fuel. This work investigates the impact of reactions between hydrogen peroxide (H_2O_2) and iron (Fe^{2+}/Fe^{3+}) on UO_2 dissolution. The reaction partners were contacted with UO_2 in oxygen-free batch reactor tests. The interaction in absence of UO_2 gives a stoichiometric redox reaction of Fe^{2+} and H_2O_2 when the reactants are present in equal concentration. Predomination of H_2O_2 results in its delayed catalytic decomposition. With UO_2 present, its dissolution is controlled by either a slow mechanism (as typical for anoxic environments) or uranium peroxide precipitation, depending strongly on the reactant ratio. Uranium peroxide ($UO_4 \cdot nH_2O$, *m*-studtite), detected on UO_2 surfaces after exposure to H_2O_2, was not found on the surfaces exposed to solutions with stoichometric Fe(II)/H_2O_2 ratios. This suggests that H_2O_2 was deactivated in redox reactions before a formation of UO_4 took place. ESR measurements employing the spin trapping technique revealed only the DMPO−OH adduct within the first minutes after the reaction start (high initial concentrations of the $OH^\bullet$ radical); however, in the case of Fe(II) and H_2O_2 reacting at 10^{-4} mol/L with UO_2, dissolved oxygen and Fe^{2+} concentrations indicate the participation of further Fe intermediates and, therefore, Fenton redox activities.

Introduction

The option of geological final storage of commercial UO_2 spent nuclear fuel is currently investigated in many countries operating nuclear power reactors. However, it must be considered that, with a possible failure of barriers in such a repository, the material might come into contact with groundwater. This might include the possible corrosion of the spent fuel matrix, its disintegration, and dissolution and mobilization of radionuclides (*1*).

Most commercial spent nuclear fuels are composed of several highly radioactive elements contained within matrix material, consisting of UO_2 (*2*, *3*). The stability of solid uranium(IV) compounds in aqueous systems depends on the electrochemical environment (*4*). UO_2 is electrochemically stable in waters of reducing conditions (that is, with an $E_h < 0$ mV). However, if oxidants have an access to the UO_2 surface, a process of oxidative dissolution is induced (*5*). Actually, the radioactivity of the spent fuel material can lead to radiolysis of surrounding water. By this process, short-lived intermediate molecules (radicals), as well as H_2O_2, O_2, and H_2 are produced, thus leading to enhanced dissolution of the matrix (*6*−*8*). Some ubiquituous groundwater ions decompose H_2O_2 by redox reactions (*9*), and recent investigations show that the oxidative attack of H_2O_2 on UO_2 material develops differently in groundwater as compared to pure water (*10*). These facts lead to a complicated multi-reaction scheme that will govern the overall oxidant production at the solid−liquid interface.

Fe(II) is typically present in most deep groundwaters since several Fe-containing minerals release the element into the contacting water. It could as well be produced during chemical reactions between repository barrier materials (e.g., canisters) and groundwater by corrosion phenomena (*11*). Magnetite (Fe_3O_4) was identified in several investigations as the phase formed preferentially during Fe corrosion experiments under anoxic conditions (*11*, *12*), leading to Fe concentrations in the range of 10^{-6}−10^{-5} mol/L. The oxidation of Fe(II) by H_2O_2 occurs via a redox cycling reaction known as the Fenton mechanism (*13*−*15*). In its simplified form, it is written as involving only free iron ions with the formation of the highly reactive hydroxyl radical (reactions A and 4 in Table 1). Additionally, Fe(II) can be regenerated by the reaction of Fe(III) with the superoxide radical ($HO_2^\bullet$), which is formed from the reaction of H_2O_2 with $OH^\bullet$ (reactions 6a and 8). Yet, even as early as 1932, Bray and Gorin (*16*) postulated the formation of a tetravalent ferryl species, which is now favored to occur in dilute aqueous solutions from iron−aquo complexes (indicated in Figure 1). In Table 1 all pertinent reactions are listed in numbered sequence, with those reactions involving free Fe(II) marked with letters. Interestingly enough, a few rate constants of the ferryl species have already been determined (*17*, *18*), which can be compared with the analogous ones for free $^\bullet OH$ radicals (*19*).

Reaction A ($Fe^{2+} + H_2O_2 \rightarrow Fe^{3+} + {}^\bullet OH + OH^-$) was found in total to follow the second-order rate law $-dH_2O_2/dt = k_1(Fe(II))(H_2O_2)$. Almost no dependence on H^+ concentration was found for the value of k_1 in early investigations (*30*). However, several referenced values exist for k_1 that differ strongly, depending less on the reaction conditions (when measured) ad more on whether free iron ions or their aquo complexes are considered (*14*, *22*, *31*). The Fenton reaction is used commercially to treat wastewaters containing organic contaminants at low pH values of 3−5 in order to avoid precipitation of solid Fe(III) phases (*15*), but at near-neutral pH it was demonstrated to make use of the reactive capacity of the Fenton cycle in heterogeneous systems (containing solid Fe(III) phases and H_2O_2) (*22*, *32*). Here, the decomposition takes place mainly at the solid surface with the rate increasing with increasing pH.

The oxidation of dissolved U(IV) to U(VI) by H_2O_2 in aqueous solution (Halpern−Smith mechanism; *33*) is described by reaction 9 ($U^{4+} + H_2O_2 \rightarrow UO_2^{2+} + 2H^+$). The mechanism of the reaction differs from that which governs the oxidation of U(IV) by atmospheric O_2 (as it occurs during UO_2 dissolution in aerated solutions) and was found to proceed by the steps 10a−d, which all involve the $OH^\bullet$ radical. It is expected that $OH^\bullet$, either formed primarily by water radiolysis or by Fenton reactions with Fe(II), will have an

* Corresponding author telephone: +49-7247-951148; fax: +49-7247-951593; e-mail: amme@itu.fzk.de.
† Institute for Transuranium Elements.
‡ GSF National Research Centre.

10.1021/es040034x CCC: $30.25
Published on Web 12/02/2004

TABLE 1. Reactions Occurring during Interaction of Fe(II)/(III), H_2O_2, and $HO_2/O_2^{\bullet -}$, and U(IV) Oxidation Reactions

no.[a]	reaction	rate constant[b]	ref
(1)	$Fe(II)(aq) + H_2O_2 \rightarrow Fe(II)(H_2O_2)(aq)$	1.3×10^7	*21*
(2)	$Fe(II)(H_2O_2)(aq) \rightarrow Fe(IV)O(aq)$	$1.0 \times 10^6\ s^{-1}$	*21*
A	$Fe^{2+} + H_2O_2 \rightarrow Fe^{3+} + {}^{\bullet}OH + OH^-$	53[c]	*20*
		5.7×10^2	*22*[d]
(3a)	$Fe(II)(aq) + HO_2^{\bullet} + H^+ \rightarrow Fe(III)(aq) + H_2O_2$	1.2×10^6	*23*
(3b)	$Fe(II)(aq) + O_2^{\bullet -} + 2H^+ \rightarrow Fe(III)(aq) + H_2O_2$	1.0×10^7	*23*
(4)	$Fe(II)(aq) + {}^{\bullet}OH + H^+ \rightarrow Fe(III)(aq) + H_2O$	3.2×10^8	*24*
(5)	$Fe(IV)O(aq) + Fe(II)(aq) \rightarrow 2Fe(III)(aq)$	1.35×10^8	*21*
(6a)	$Fe(III)(aq) + HO_2^{\bullet} \rightarrow Fe(II)(aq) + H_2O_2 + H^+$	$<2.0 \times 10^3$	*23*
(6b)	$Fe(III)(aq) + O_2^{\bullet -} \rightarrow Fe(II)(aq) + O_2$	1.5×10^8	*21*
B	$Fe^{3+} + O_2^{\bullet -} \rightarrow Fe^{2+} + O_2$	3.1×10^7	*22*[d]
(7a)	$Fe(III)(aq) + H_2O_2 \rightarrow Fe(III)(OH)(HO_2)^+ + H^+$	2×10^{-4}	*26*
(7b)	$Fe(III)(OH)(HO_2)^+ \rightarrow Fe(II)(aq) + HO_2^{\bullet}$	$2.7 \times 10^{-3}\ s^{-1}$	*27*
C	$Fe^{3+} + H_2O_2 \rightarrow Fe^{2+} + HO_2^{\bullet} + H^+$	2.6×10^{-3}	*22*[d]
(8)	$H_2O_2 + {}^{\bullet}OH \rightarrow HO_2^{\bullet} + H_2O$	3.0×10^7	*19*
(9)	$U^{4+} + H_2O_2 \rightarrow UO_2^{2+} + 2H^+$	1.2−2.5	*28*
(10a)	$U(IV) + H_2O_2 \rightarrow U(V) + OH^{\bullet}$		*28*
(10b)	$U(V) + H_2O_2 \rightarrow U(VI) + OH^{\bullet}$		*28*
(10c)	$U(IV) + OH^{\bullet} \rightarrow U(V) + H_2O$		*28*
(10d)	$U(V) + OH^{\bullet} \rightarrow U(VI) + H_2O$		*28*
(11)	$U(IV) + 2Fe^{3+} \rightarrow U(VI) + 2Fe^{2+}$	pH dependent	*29*

[a] Lettered reactions in italics with free iron species. [b] Dimension of all rate constants, except 2 and 7b, are $dm^3 \cdot mol^{-1} \cdot s^{-1}$; the exceptions are first-order reactions with dimension s^{-1}. [c] *V*alue is average of 15 values from the literature. [d] Rate constants determined at pH 5; values at pH 3 and 4 are also listed.

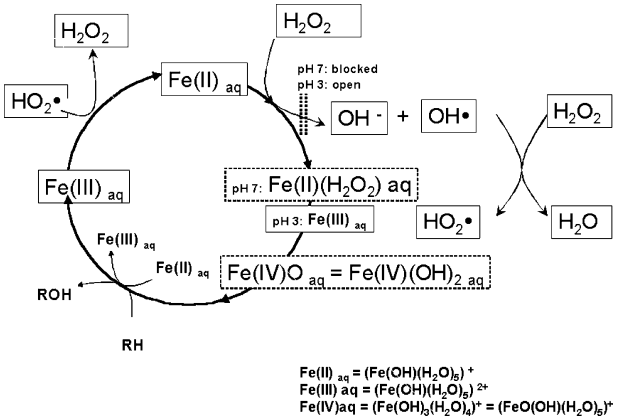

FIGURE 1. Schematic diagram of redox cycling reactions in a system containing Fe(II) and H_2O_2 (Fenton-like reactions).

influence on the rate of the UO_2 dissolution during the reaction of U(IV) with H_2O_2. At higher peroxide concentrations, the precipitation of uranium peroxide (*10*, *34*) is expected to compete with Fenton reactions:

$$UO_2^{2+} + H_2O_2 + H_2O \rightarrow UO_4 \cdot (nH_2O) + 2H^+ \quad (12)$$

Uranium peroxide formed by this reaction was measured to have solubilities in the order of 10^{-7} mol/L at pH 3.1−3.7 and $[H_2O_2] = 10^{-3}$ M (*35*).

The purpose of this study was to investigate the influence of Fe(II) and H_2O_2 interaction upon the dissolution of UO_2. Although the electrochemical model describing the anodic UO_2 dissolution is well accepted (*5*), relatively few studies have examined systematically the relations between UO_2 dissolution kinetics and reaction product formation in natural systems. We present here data from batch-reactor experiments conducted with reactant concentrations similar to those expected to appear under nominally anoxic repository conditions (*5*, *12*). By comparing the measurements with calculations using a set of parallel concurring reactions, we (i) quantify the formation of reaction products formed via the different reaction routes and (ii) determine concentration thresholds that separate the reaction pathways.

Experimental Section

Materials. The kinetic tests were conducted in glass vessels after purging with Ar of high purity (2 ppm O_2). Pellets of freshly reduced depleted UO_2 (weight approximately 1.2 g) were used as solid phase for the experiments. The leaching solutions were prepared from deionized water/KCl (3 mmol/L). Fe^{2+} was added as solution of $FeSO_4 \cdot 7H_2O$ (Merck, p.a. grade). H_2O_2 solutions were prepared from a H_2O_2 stock solution (34%, Merck, p.a. grade).

Measurement of Hydrogen Peroxide. Hydrogen peroxide was analyzed with the DPD method (*36*). Analysis was performed by obtaining a zero value at the measurement wavelength (528 nm) and measuring subsequently the sample after mixing with the test substance. The determination limit of the method (the way it was used here) is given to 5.9×10^{-7} mol/L H_2O_2.

Measurement of Iron. The PPST/Ferrozine method was used for Fe(II) and Fe(III) measurements (*37*). The detection limit of the method is given at 3.6×10^{-7} mol/L Fe.

Measurement of Uranium. U was determined by inductively coupled plasma mass spectrometry (ICP-MS, ThermoFinnigan Element 2) installed in a glovebox. Initially, a semiquantitative survey of all samples was done to establish the approximate uranium concentrations to estimate appropriate dilutions to match the instrument. Each sample was then measured in triplicate (detection limit of the method at 4×10^{-12} mol/L U).

Kinetic Experiments and Control of Solution Parameters. A Mettler Toledo 4805 Au electrode and WTW Multilab P 5 measurement unit were used for redox control. Au was chosen as electrode material in order to avoid decomposition of trace amounts of H_2O_2 in solution by catalytic activity of Pt surfaces. Dissolved oxygen was determined using a WTW TriOximatic sensor (detection limit $[O_2]_{diss} = 0.01$ mg L^{-1}). To establish anoxic conditions, Ar (nominal oxygen content 2 ppm) was purged through the solutions prior to the experiments, and the experimental apparatus was placed in an Ar glovebox. The reactant solutions were prepared with deaerated deionized water inside the box. After starting the experiment, Ar purging was stopped in order to prevent the reacting solution from vaporization and to avoid introduction of trace oxygen. The fractions sampled for U analysis were

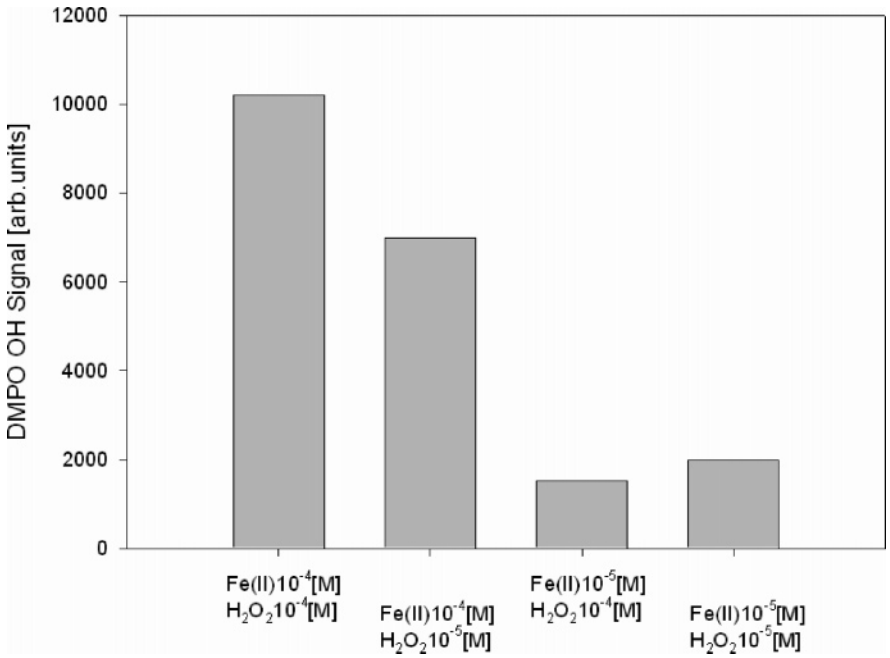

FIGURE 2. Yield of the DMPO−OH signal at the concentrations ratios indicated.

not filtered intentionally since we were interested in measuring the total U in the system, which is made up by the dissolved fraction and by the fraction bound to precipitated iron oxyhydroxyde phases. For the fractions sampled after long reaction times, a filtration through 20 nm was done in order to study the fraction of U bound to precipitates. The filtered solid was dissolved and analyzed for [U] and [Fe]. A fraction between 3.1% and 25.2% of the total uranium suspended in the reacting solutions was found on the Fe precipitates.

Surface Analysis with SEM-EDX. After each experiment the solid phases were rinsed with a small volume of deionized water to remove residuals of the leaching solutions and afterward dried for 7 d in a mild vacuum. Examination with SEM-EDX was performed with a Philips SEM 515 scanning electron microscope with an acceleration voltage of 30 kV, using a Tracor detector for the EDX measurements.

ESR Measurements. The ESR experiments were carried out on a Bruker 300ESP spectrometer with the following settings: modulation amplitude 1 G, scan speed 2.5 G/s, power 20 mW, gain 5×10^4, X-band at 9.75 GHz. The spin-trap method using DMPO (5,5-dimethyl-1-pyrrolidine *N*-oxide) was applied to obtain stronger signals of the OH• radical. Two experimental approaches were used: (i) the Fenton reaction, after initiation by the final addition of H_2O_2, was run for 1 min before the addition of DMPO at a final concentration of 10 mM; (ii) DMPO was added either before the start of the Fenton reaction or at various times afterward. In each case the scans were started 2 min later. Fluorescence emission of hydroxylated terephthalate was measured at 435 nm after excitation at 323 nm (*38*) in the flow-through cell (3 μL active volume) of the LS30 fluorescence detector (Perkin-Elmer, Germany).

Results

ESR Measurements. The production of radical intermediates in solutions of H_2O_2 and Fe(II) was evaluated by the ESR/spin-trapping technique. Unfortunately, the spin-trap DMPO does not distinguish between free •OH radicals or the ferryl species. Yet, in the dilute aqueous solution we assume that iron is present as hexa-aquo complex and that the subsequent reactions ultimately lead to the ferryl species (*20*, *21*, *39*−*41*). Another radical potentially formed during the reaction sequence $^{-}HO_2^{\bullet}/O_2^{\bullet-}$ from the reaction of •OH with excess $H_2O_2^{-}$ is unlikely to be observable by the EPR/spin-trapping method due to the slow trapping reaction and its far lower steady-state concentration. Other competing reactions $HO_2^{\bullet}/O_2^{\bullet-}$ could undergo are its disproportionation, its very slow reaction with excess H_2O_2 or with Fe(III).

In the reaction with both reactants present at 10^{-5} M, the DMPO−OH signal is only 20% of that at 10^{-4} M, as can be seen in Figure 2. For the other two ratios of reactants, differences were found. With Fe(II) present at 10^{-4} M, the signal intensity is close to that produced during the reaction of Fe(II) and H_2O_2 at 10^{-4} M. In contrast, if the ratio is exchanged (that is, with Fe(II) at 10^{-5} and H_2O_2 at 10^{-4} M), the signal is lowest of all cases but close to the one of Fe(II)/H_2O_2 at 10^{-5} mol/L. This indicates that the rate of •OH or ferryl production is mainly dependent on the concentration of Fe(II) and less so on the H_2O_2 concentration. We calculated [•OH] for our systems with the numerical kinetic reaction code MACKSIMA-CHEMIST, using reaction rate data compiled in a recent publication (*42*) to introduce a dimension into the relative values of the ESR determinations. The results predict [•OH] ratios in-between the systems very similar to our experimental results, with absolute values of about 10^{-12} mol/L [•OH] at the beginning and dropping below 10^{-16} mol/L after 100 min.

Additionally, the •OH/ferryl yield was determined for [H_2O_2] and [Fe(II)] equimolar at 10^{-4} M over a time period of up to 10 min (Figure 3), in which case the spin-trap was added at the times plotted in this figure.

The time dependence of the formation of the spin adduct shows that the reactive species disappear(s) almost completely within that period. Preliminary tests in air-saturated water showed no relevant difference in the ESR intensities to those presented here, proving that the Fenton chemistry in these systems during short reaction times is not affected by the presence of oxygen. All further studies were carried out in Ar-saturated aqueous solutions.

Looking at longer observation times for a potential recurrence of Fe(II) according to reactions 6a or 6b, even with the incremental addition of H_2O_2, no reemergence of the DMPO−OH signal was observed, neither could we see any traces due to the depletion of a DMPO−OOH adduct during our observation period of maximally 48 h, which was

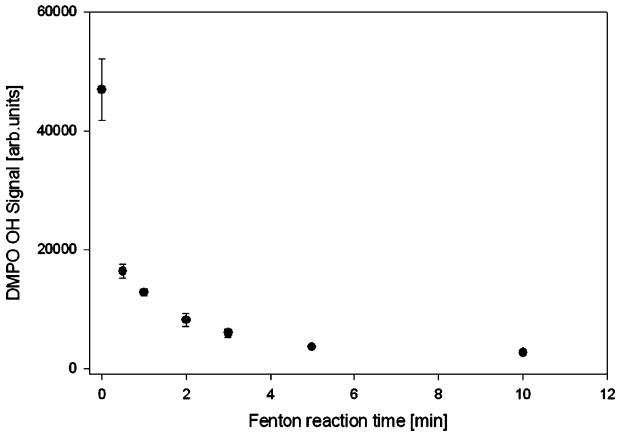

FIGURE 3. Depletion kinetics of the DMPO−OH signal in the Fenton system.

shorter than the period used in the other experiments. The fact that the spin adduct of DMPO−OOH is far less stable than that of DMPO−OH and that it decays into the latter species (*43*) makes it unlikely that the disappearance of $HO_2^{\bullet}/O_2^{\bullet-}$ can be observed at all. Indeed, during all our ESR measurements, we were never able to detect other signals aside from the DMPO−OH adduct; therefore, a transient appearance of $HO_2^{\bullet}/O_2^{\bullet-}$ cannot be ruled out.

Batch Experiments on the Decomposition of H_2O_2 and Oxidation of Fe(II) to Fe(III). Before testing the simultaneous influence of Fenton-like systems on UO_2 dissolution, the reaction kinetics of Fe(II) with H_2O_2 alone were investigated. We measured in the concentration ranges relatively low as compared to those of related studies, for these are relevant for repository conditions. In addition, oxygen-free conditions were maintained. Kinetic profiles of H_2O_2 decomposition and Fe(II) to Fe(III) oxidation were measured by recording concentrations during batch tests containing Fe(II) and H_2O_2 in the concentration ratios given in Table 2. A kinetic rate law of second order (using reaction A: $Fe^{2+} + H_2O_2 \rightarrow Fe^{3+} + {}^{\bullet}OH + OH^-$) was applied to obtain a fit on the experimental data.

With both reactants present at 10^{-5} mol/L, Fe could only be detected as Fe(III) in the first phase of the reaction. For longer reaction times, Fe(III) concentration dropped below the detection level due to the formation of solid iron oxyhydroxides by hydrolysis and precipitation. In the experiment having Fe(II) present at 10^{-4} mol/L and H_2O_2 present at 10^{-5} mol/L, Fe concentrations remained close to the starting value during the reaction and H_2O_2 was consumed almost immediately. In the experiment with H_2O_2 at 10^{-4} mol/L and Fe(II) present at 10^{-5} mol/L, the H_2O_2 concentration remained almost unchanged during the reaction until 1200 min passed, due to its excess; however, H_2O_2 could not be measured after 10^4 min. This is explained by catalytic decomposition of H_2O_2 at surfaces of precipitated iron oxihydroxides after long reaction times (*32*). In this system, Fe concentrations are decreasing by precipitation of solid iron oxides (which could be observed in the vessel) until not detectable after 1000 min. In the experiment with 10^{-4} mol/L for both reaction partners, concentrations of Fe develop unexpectedly because after long reaction times (longer than 8×10^4 min) almost equal amounts of Fe(II) and Fe(III) were found in solution, but at intermediate reaction times Fe(II) was not found; instead, a precipitation of brown solid iron oxyhydroxyde phases was observed. These disappeared later for the most part. Together with the consumption of H_2O_2 at this reaction time, the observations indicate that Fe(II) was regenerated in solution by reaction of H_2O_2 with the solid Fe(III) precipitate or by homogeneous reaction with dissolved Fe(III).

Batch Experiments on the Reactions UO_2−H_2O_2. The dissolution of UO_2 in oxygen-free aqueous solution containing H_2O_2 was measured as function of time in order to understand the kinetics of the interaction in the absence of the third reaction partner, Fe. Dissolution kinetics were measured for UO_2 in deaerated 10^{-4} and 10^{-5} M H_2O_2 solution. A second-order kinetic rate law was applied to obtain a fit on the experimental values (shown in Figure 4). However, the dissolution reaction taking place during the experiment is more complicated than the electron transfer between dissolved reactants in a homogeneous system. This situation required the simplification of the kinetic treatment for uranium oxidation, which will be explained in the following.

Reaction 9 ($U^{4+} + H_2O_2 \rightarrow UO_2^{2+} + 2H^+$) obeys a second-order rate law for the decrease of U(IV) in solution, but determination of the dissolved U(IV) fraction is difficult. For the calculations done here, it was assumed that all uranium dissolved during the experiment (by H_2O_2-induced oxidation) is present as U(VI) (uranyl). U(VI) under the conditions at the end of the experiment (positive E_h, very low $[CO_3^{2-}/HCO_3^-]$, near-neutral pH) is in equilibrium with the solid phases of the schoepite class ($(UO_2)_8O_2(OH)_{12}(H_2O)_n$, $n = 10$ or 12), which are known to have a solubility in the order of 10^{-4} mol/L under ambient geochemical conditions (*44*). Following these conditions, the maximum $[U]_{diss}$ at the end of the experiment would be 10^{-4} mol/L, giving therefore the upper limit for the application of the kinetic model ($[U]_{diss}$ in equilibrium with uranyl peroxo minerals were reported to be lower; *35*). However, if the dynamic situation of dissolving UO_2 is expressed as static batch reaction between dissolved reactants, we have to imply that initially 10^{-4} mol/L U(IV) are present, which can convert to U(VI). This is not possible from the standpoint of solution thermodynamics (since the maximum concentration of U(IV) is given by UO_2 solubility, being below the schoepite minerals solubility). We assume here a formation of U(VI) by surface complexation with the oxidant (*45*), then the amount of U(IV) becomes dependent from the exposed reactive surface sites but is virtually unlimited (the source being the crystal lattice of UO_2); hence, the condition of 10^{-4} mol/L U(IV) is fulfilled. The mechanisms used here differ from those assumed in electrochemical models, which explain UO_2 dissolution as anodic process, driven by its semiconductor nature (*5*).

The fit resulting from a law of first order (shown in Figure 4) is used in a parallel kinetic model in the next section. The rate constants found for a second-order law are close to those given by Baker and Newton (*28*) (see Table 2).

Batch Experiments on the Reactions Fe(II)−H_2O_2−UO_2. To study the interactions of the three reaction partners, the combinations given in Table 3 were investigated by monitoring the concentrations of U, Fe(II), Fe(III), and H_2O_2 as a function of time. The concentrations determined by experiments are shown in Figure 5a−c. A thermodynamic calculation was performed with the code PHREEQC and the NEA uranium database (*44*) in order to determine the dominant dissolved U species at the beginning (anoxic conditions, $[Fe^{2+}]$, $[SO_4^{2-}] = 10^{-5}$ mol/L]) and at the end (oxic conditions) of the experiments. The result is shown in Figure 5d; arrows indicate the shift of the geochemical parameters from $E_h =$ +50 mV to +650 mV (as was measured versus the standard H_2 electrode). The calculations predict only hydroxo species to be present in higher percentages, and experiments are calculated to start with mainly U(IV) dissolved (before H_2O_2 addition), which is then oxidized to U(VI).

Uranium concentrations were found to behave different in each of the tests. For the system $Fe_4/P_4/UO_2$, U concentrations are increasing steadily with time, and the maximum concentration measured after about 10^4 min is in the range of 10^{-4} mol/L, typical for aerated systems of dissolving UO_2 in equilibrium with the schoepite-type phases. For the system

TABLE 2. Reactant Ratios and Fitted Kinetic Constants (Determined from Experiments in This Work) for Reactions of Fe(II) with H_2O_2 and UO_2 (U^{4+}) with H_2O_2

combination of reactants	expt label	reaction rate	k_1 (s^{-1}) k_2 (M^{-1} s^{-1})
$[H_2O_2] = 10^{-5}$ mol/L:[Fe(II)] = 10^{-5} mol/L	Fe5P5	1	2×10^{-2}
		2	2.89×10^{6}
$[H_2O_2] = 10^{-4}$ mol/L:[Fe(II)] = 10^{-5} mol/L	Fe5P4	1	5×10^{-3}
		2	5.33×10^{6}
$[H_2O_2] = 10^{-5}$ mol/L:[Fe(II) = 10^{-4} mol/L	Fe4P5	1	$2{,}75 \times 10^{-2}$
		2	2.89×10^{6}
$[H_2O_2] = 10^{-4}$ mol/L:[Fe(II) = 10^{-4} mol/L	Fe4P4	1	4.5×10^{-2}
		2	5.55×10^{4}
$[H_2O_2] = 10^{-5}$ mol/L + solid UO_2	UO2P5	1[a]	9×10^{-7}
		2[a]	1.7
$[H_2O_2] = 10^{-4}$ mol/L + solid UO_2	UO2P4	1[a]	5×10^{-7}
		2[a]	0.5

[a] This constant was determined according to the homogeneous U^{4+} oxidation reaction, as mentioned in the text.

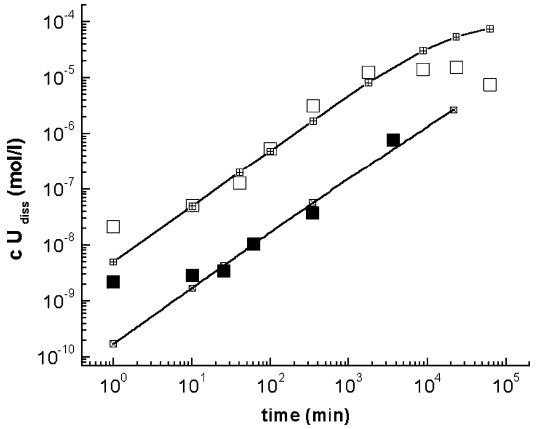

FIGURE 4. Experimentally determined concentration (mol/L) of dissolved U during the reaction of UO_2 with (i) 10^{-4} and 10^{-5} mol/L and (ii) deaerated H_2O_2 solution, in comparison with the calculated concentration using a rate law of first order: $C_{U(VI)} = C_{eq,U(VI)} - (C_{0\ U(IV)}e^{-kt})$ (with $C_{U(VI)}$ = resulting $[U(VI]_{diss}$, $C_{eq,U(VI)}$ = maximum equilibrium $[U(VI]_{diss}$, and $C_{0,U(IV)}$ = initial [U(IV] for conversion). (□) Measured UO_2 (cr) in $[H_2O_2] = 10^{-4}$ mol/L; (■) measured UO_2 (cr) in $[H_2O_2] = 10^{-5}$ mol/L; (⊞, X inside a box) model fitting of $[U]_{diss}$ using the constants given in Table 2 (UO_2P_4 and UO_2P_5, respectively).

$Fe_5/P_4/UO_2$, the same trend is observed for U up to 5000 min of reaction time; afterward, U concentration is decreasing due to the onset of the precipitation of a secondary product, which most obviously consists of uranium peroxide ($UO_4 \cdot xH_2O$), as it was found by the SEM examination. The low uranium concentration (about 10^{-7} M) resulting was only expected for $[H_2O_2]$ higher than 10^{-4} M. An explanation based on the sorption of U on iron oxide precipitation products seems to be unlikely: these precipitates formed during the experiment were taken into account when measuring uranium. For the system $Fe_5/P_5/UO_2$, much lower U concentrations in solution (of the order of 10^{-8} mol/L) are observed after 10^4 min of reaction time. Such concentrations are observed typically with UO_2 dissolving in nominally anoxic (deaerated) solutions and were recently measured in the presence of iron corrosion products under anoxic conditions (*46*). H_2O_2 could not be measured after 300 min in the system $Fe_4/P_4/UO_2$ and was consumed immediately in the system $Fe_5/P_5/UO_2$. In the system $Fe_5/P_4/UO_2$, it was detected after more than 10^4 min (then close to detection limit).

The behavior of Fe in system $Fe_4/P_4/UO_2$ is different than the observations made for the other experiments: the initial concentration of Fe(II) (10^{-4} mol/L) is decreasing steadily until it falls below the detection limit after 100 min (indicated as data points in brackets); however, after 10^4 min it is detected again, proving that Fe(II) was regenerated in the reacting system; simultaneously, dissolved oxygen concentration increases. The behavior is explained by the formation of $HO_2^\bullet$ from Fe^{3+} and H_2O_2 (following reaction C), its subsequent conversion to $O_2^{\bullet -}$, and the resulting formation of Fe(II) and O_2 (reaction B) with $HO_2^\bullet$ and H_2O_2 steady-state concentrations too low to be detected. For the other systems, enhanced oxygen concentrations and subsequent consumption were found after short reaction times (Figure 6). In these cases, the concentration of dissolved Fe(III) becomes too low for O_2 production resulting from reactions $Fe^{2+} + H_2O_2 \rightarrow Fe^{3+} + {}^\bullet OH + OH^- \rightarrow (+H_2O_2)HO_2^\bullet + H_2O \rightarrow (+Fe^{3+}) \rightarrow Fe^{2+} + O_2$ (A−(8)−B) after long reaction times. It was found also that the extent of regeneration is higher in the system with solid UO_2 than during the homogeneous reaction of the dissolved reactants H_2O_2 and Fe(II): in the latter case, only 20% of total Fe (50% of all Fe dissolved at long reaction times) is present as Fe(II). A similar observation was made during the dissolution of uranium dioxide in acidic solutions (*47*) and proves that U is contributing to the reduction of Fe. Concentrations of dissolved oxygen after longer times were found to be lower for the homogeneous than for the heterogeneous system, proving also the participation of U(IV) in the Fenton reaction.

Surface Investigation with SEM-EDX. The UO_2 surfaces were examined with SEM-EDX for surface alterations and formation of secondary phases after the leaching process. Samples treated in solutions containing the same order of concentration of peroxide and Fe show an intact UO_2 grain structure for the greatest part (see Figure 7a,b). The surface obviously has not suffered heavy damage, as it is often observed with, for example, leaching in oxidizing solutions. Only few, noncrystalline alteration products were found on the surfaces, containing uranium as the only element detectable with EDX; these observations allow us to conclude that Fe was neither coprecipitated nor sorbed in significant amounts during the leaching process. However, very thin sorbed layers cannot be detected with the EDX technique used here. When H_2O_2 was used in excess (at 10^{-4} mol/L) and Fe(II) was present with 10^{-5} mol/L, the surface of the UO_2 samples was covered almost completely with fine acicular crystals (shown in Figure 7c). These objects have a length of approximately 50 nm and a diameter of a few nanometers. This compound is very probably uranium peroxide (studtite, $UO_4 \cdot 4H_2O$, or *m*-studtite with $2H_2O$) since crystal arrangements of identical habitus were found on samples that were treated with solutions containing peroxide only (Figure 7d). The precipitation takes place after about the same reaction times for experiments with and without Fe(II). Ferric oxides that were produced during reaction with

TABLE 3. Reactant Ratios Used in UO_2 Dissolution Experiments in Presence of Fe(II) and H_2O_2 and Kinetic Constants Applied for the First-Order Parallel Kinetics Scheme

combination of reactants	expt label	pH development	reaction rate used in kinetic evaluation	$k_{FeOxidation}$ (s^{-1}) $k_{U\ Oxidation}$ (s^{-1})
$[H_2O_2] = 10^{-5}$ mol/L:[Fe(II)] = 10^{-5} mol/L + solid UO_2	UO2Fe5P5	5.3 → 5.6	first-order parallel reaction scheme, reactions *A* and 9	2×10^{-2} 9×10^{-7}
$[H_2O_2] = 10^{-4}$ mol/L:[Fe(II)] = 10^{-5} mol/L + solid UO_2	UO2Fe5P4	5.5 → 7.0		5×10^{-3} 9×10^{-7}
$[H_2O_2] = 10^{-4}$ mol/L:[Fe(II)] = 10^{-4} mol/L + solid UO_2	UO2Fe4P4	4.2 → 4.2		4.5×10^{-2} 5×10^{-7}

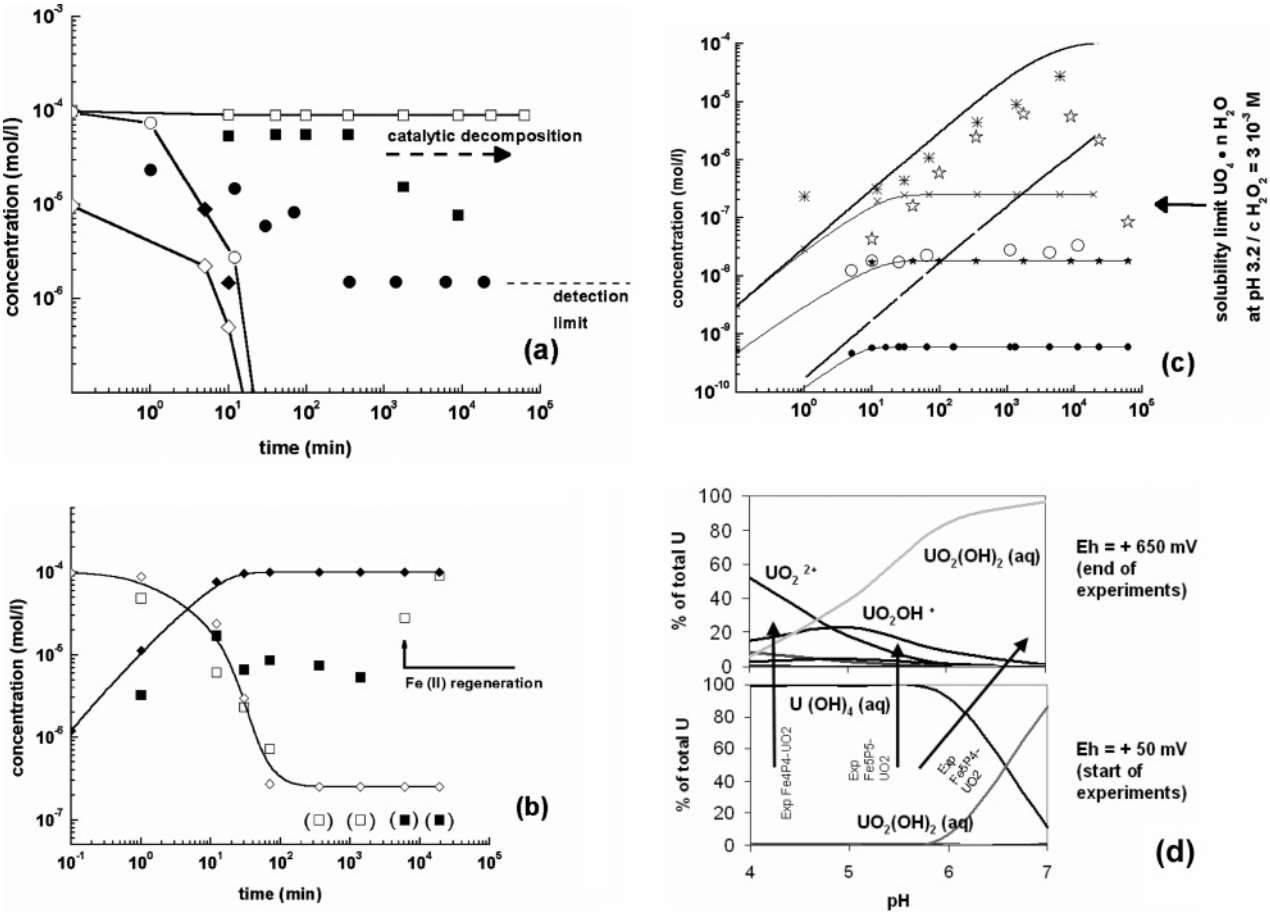

FIGURE 5. (a–d) Experimentally determined concentrations (data points) in the experiments with H_2O_2–Fe(II)–UO_2 and results of modeling calculations with parallel reaction kinetics (law for parallel concurring reactions of 1st order, lines). (a) $[H_2O_2]$: (●) measured in the system UO_2 (cr) with [Fe(II)] = 10^{-4} mol/L and $[H_2O_2] = 10^{-4}$ mol/L; (◆) measured in the system UO_2 (cr) with [Fe(II)] = 10^{-5} mol/L and $[H_2O_2] = 10^{-5}$ mol/L; (■) measured in the system UO_2 (cr) with [Fe(II)] = 10^{-5} mol/L and $[H_2O_2] = 10^{-4}$ mol/L; (–○–) model prediction for UO_2 (cr) in [Fe(II)] = 10^{-4} mol/L and $[H_2O_2] = 10^{-4}$ mol/L, obtained by using parallel (concurring) kinetics (rate constants used in model prediction given in Table 3); (–◇–) model prediction for UO_2 (cr) with [Fe(II)] = 10^{-5} mol/L and $[H_2O_2] = 10^{-5}$ mol/L; (–□–) model prediction for UO_2 (cr) with [Fe(II)] = 10^{-5} mol/L and $[H_2O_2] = 10^{-4}$ mol/L. (b) [Fe(II)/(III)] in the experiments with 10^{-4} mol/L H_2O_2 and 10^{-4} mol/L Fe(II): (□) measured [Fe(II)]; (■) measured [Fe(III)]; (–◇–) model prediction for [Fe(II)]; (–♦–) model prediction for [Fe(II)]. (c) $[U]_{diss}$: (∗) measured in the system UO_2 (cr) with [Fe(II)] = 10^{-4} mol/L and $[H_2O_2] = 10^{-4}$ mol/L; (☆) measured in the system UO_2 (cr) with [Fe(II)] = 10^{-5} mol/L and $[H_2O_2] = 10^{-4}$ mol/L; (○) measured in the system UO_2 (cr) with [Fe(II)] = 10^{-5} mol/L and $[H_2O_2] = 10^{-5}$ mol/L; (–×–) $[U]_{diss}$ in solutions with [Fe(II)] = 10^{-4} mol/L and $[H_2O_2] = 10^{-4}$ mol/L, calculated by using parallel (concurring) kinetics (constants given in Table 3); (–●–) $[U]_{diss}$ in solutions with [Fe(II)] = 10^{-5} mol/L and $[H_2O_2] = 10^{-5}$ mol/L, calculated by using parallel (concurring) kinetics (constants given in Table 3); (–★–) $[U]_{diss}$ in solutions with [Fe(II)] = 10^{-5} mol/L and $[H_2O_2] = 10^{-5}$ mol/L, calculated by using parallel (concurring) kinetics (constants given in Table 3); solid and dashed line, no symbol: modeled values of $[U]_{diss}$ in solutions containing H_2O_2 but no Fe(II) (10^{-4} and 10^{-5} mol/L, respectively), using the constants given in Table 2. (d) Dissolved species distribution for U at beginning and end of the experiments (calculated with a low ionic strength model for dissolving UO_2 with [Fe^{2+}, SO_4^{2-}] = 10^{-5} mol/L].

H_2O_2 were not coprecipitated during the formation of $UO_4 \cdot xH_2O$.

Kinetic Modeling of Parallel Reactions. It was investigated if the simultaneous reaction of U^{4+} (originating from dissolving UO_2) and Fe(II) with H_2O_2 in aqueous systems can be described, with some simplifications, as a system of two concurring parallel reactions using homogeneous kinetic rate laws. The use of a set of "classical", analytical rate laws has advantages when monitoring the reaction progress. Reactions were formulated as competitive parallel pseudo-first-order reactions of the general type A → D + ... (k_1), A → E + ... (k_2), with rate laws $-dc_A/dt = k_1c_A + k_2c_A$, $dc_D/dt = k_1c_A$, and $dc_E/dt = k_2c_A$, resulting in expressions for concentrations after integration of the laws. Using k_A and k_9 for k_1 and k_2,

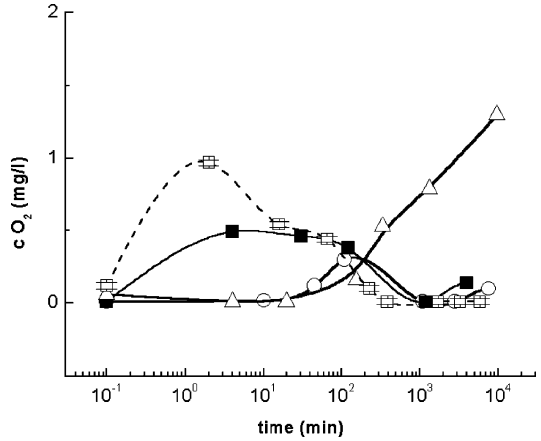

FIGURE 6. Concentrations of dissolved oxygen (mg/L) during the reaction of UO_2 with H_2O_2 and Fe(II) in the three different ratios selected. For comparison, results of one of the experiments without UO_2 are shown: (○) UO_2 (cr) in [Fe(II)] = 10^{-5} mol/L and [H_2O_2] = 10^{-5} mol/L; (■) UO_2 (cr) in [Fe(II)] = 10^{-5} mol/L and [H_2O_2] = 10^{-4} mol/L; (△) UO_2 (cr) in [Fe(II)] = 10^{-4} mol/L and [H_2O_2] = 10^{-4} mol/L; (□) [Fe(II)] = 10^{-4} mol/L and [H_2O_2] = 10^{-4} mol/L, no solid phase.

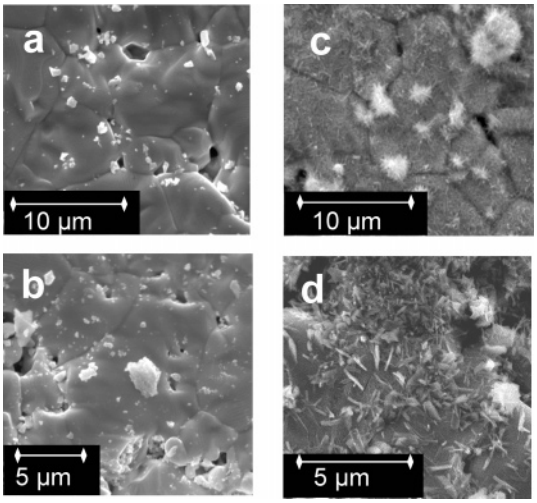

FIGURE 7. SEM micrographs of the UO_2 surfaces leached in different solutions: (a) 10^{-5} M Fe(II)/10^{-5} M H_2O_2; (b) 10^{-4} M Fe(II)/10^{-4} M H_2O_2; (c) 10^{-5} M Fe(II)/10^{-4} M H_2O_2; (d) no Fe(II)/10^{-4} M H_2O_2.

respectively, the resulting algebraic expressions for the concentrations in the specific case are as follows:

$$c_A = c_{A,0} \exp[-(k_A + k_9)t]$$

$$c_D = c_{D,0} + c_{A,0}k_A/(k_A + k_9)\{1 - \exp[-(k_A + k_9)t]\}$$

$$c_E = c_{E,0} + c_{A,0}\, k_A/(k_A + k_9)\{1 - \exp[-(k_A + k_9)t]\}$$

Rate constants as given in Table 3 were used for the calculations with the parallel reaction model. The resulting data for $[U]_{diss}$, [Fe(II)/(III)], and [H_2O_2] are shown as solid lines in Figure 5a−c. Figure 8a displays how the kinetic reaction path is controlled by the ratio of the concurring reactions constants: the plot presents the consumption of H_2O_2 that proceeds (in a generalized way) by the two reactions I (oxidation of Fe(II)) and II (oxidation of U(IV)). With a ratio of rate constants = 1, both reactions contribute equally to H_2O_2 consumption; with one reaction of the parallel scheme faster than the other, the ratio is different from 1 (indicated by lines). In the present case, the Fe(II)−H_2O_2 reactions proceeds faster than the oxidation of UO_2(cr) as indicated by the arrow.

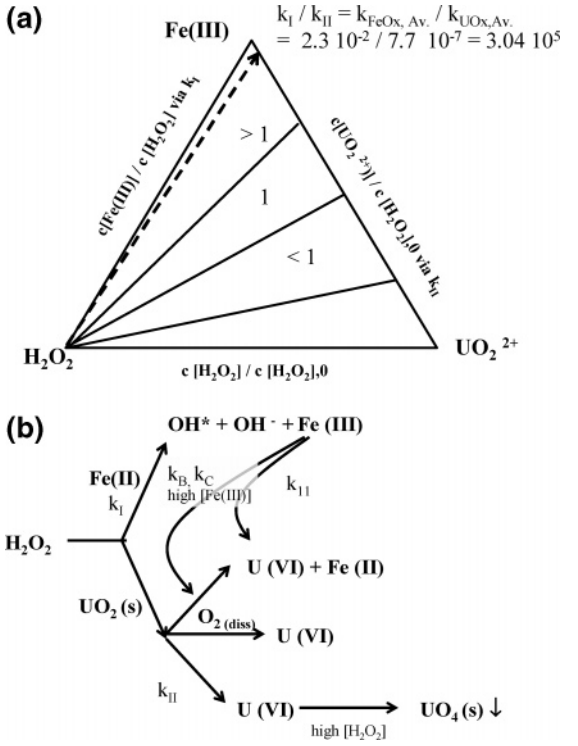

FIGURE 8. Parallel reaction scheme of the solution reactions considered for the heterogeneous system Fe(II)−H_2O_2−UO_2(s). The ratio of averaged reaction constants is displayed by the arrow (see text for explanation). (b) Proposed reactions pathways of Fe and U redox conversion.

The parallel reaction scheme describes the decrease of Fe(II) by oxidation and the decomposition of H_2O_2 sufficiently (with some overprediction of reaction times). The reformation of Fe(II), as was observed, is not predicted by the model since the reactions that are supposed to be responsible for it were not included. Uranium concentrations predicted on the base of UO_2(s)−H_2O_2 reactions alone do not coincide with those experimentally determined for the heterogeneous systems $Fe_4/P_4/UO_2$ and $Fe_5/P_5/UO_2$, thus confirming that Fe(II) influences U dissolution. Initially (for the first minutes of reaction in which H_2O_2 is present abundantly), the U concentration is calculated by the parallel kinetic scheme to increase and then to remain on a plateau level since H_2O_2 is much more quickly consumed by Fe oxidation than by U oxidation.

For the case of $Fe_5/P_4/UO_2$, the experimental data follow closely the relation found for UO_2 dissolution in pure H_2O_2 solutions (without Fe present) at shorter reaction times, which is due to the excess of H_2O_2. The amount of U dissolved by the parallel reaction is small since the competitive scheme including Fe contributes only in the early stage of the reaction. For the case of the system $Fe_4/P_4/UO_2$, uranium dissolution proceeds further after H_2O_2 was consumed and continues up to the order of uranium(VI) oxyhydroxyde solubility values due to dissolved oxygen (or interaction with strongly oxidizing intermediate species) formed during the Fenton reaction. Here, also, the fraction dissolved as consequence of the parallel reaction is small.

In the system $Fe_5/P_5/UO_2$, it was found that the development of uranium concentration differs from those of the test with peroxide alone (UO_2/P_5). The prediction of the parallel reaction scheme describes the dissolution data better than the rate law found for dissolution in pure H_2O_2, although underestimated by more than 1 order of magnitude. For this system, the concept of the concurring parallel reactions reproduces the trend of observed data and

was able to best explain the development in U dissolution values.

Discussion

The redox cycling of iron via radical-controlled Fenton-like reactions and the oxidative dissolution of UO_2 to U(VI) are, in view of material stability, among the crucial chemical reactions expected to occur at the UO_2 surface under geologic repository conditions. The experimental data obtained from the measurement of [H_2O_2], [Fe(II/III)], and [U] suggest that the chemical reaction path of the reactants (and, as a consequence, the mobilization of uranium) depends strongly on the ratio of the partners. A catalytic decomposition of H_2O_2 on solid Fe phases surfaces, as observed in preliminary tests, proved to be slow enough to allow excess H_2O_2 to react with solid UO_2 and precipitate uranium peroxide, as proved by SEM. This, in turn, leads to the unexpected result of lowered dissolved U concentration in the presence of a strong oxidant (H_2O_2). The re-formation of Fe(II) in the reacting solution at 10^{-4} M is coupled with strong enhancement of $[U]_{diss}$ after consumption of peroxide, which is an evidence for the impact of the Fenton chemistry on UO_2 dissolution. Figure 8b proposes a scheme of how the several relevant reactions contribute to the redox chemistry. The evaluation with the parallel kinetics law model demonstrates that secondary reactions (typically appearing during radical redox cycles) can lead to unexpected effects on the UO_2 dissolution.

Further possible factors of influence should be discussed: reaction A was reported to be independent of pH (*30*), and reaction 9 was found to depend only weakly on pH. Therefore, the two reactions were used in the parallel reaction scheme without a correction for pH shifts. However, very different rate constants were reported by other investigators for reaction A, showing a strong dependence on pH (given in Table 1). For further elaboration of the reaction scheme, the dependence on [H^+] needs to be taken into account.

Reaction 9, which was used here to describe UO_2 oxidation, is a simplification that may be acceptable for the purpose of this study. In further interpretations, it has to be taken into account that the concentration of U(IV) in repository systems is linked to the dynamic dissolution of UO_2. During this process, U(IV) is delivered continuously into solution, following rate laws that describe the dissolution by mass release as function of time and surface area. Such an expression will have to be coupled to the source term of U(IV) concentration in solution in order to take into account realistic spatial gradients in dissolution experiments.

Additionally, the production of H_2O_2 (or radical species) by water radiolysis resulting from radioactive decay will create reaction patterns different from the static systems investigated here. In the real case, H_2O_2 is produced continuously by the radiation field and delivered into the solution. Such a dynamic system will depend strongly on the reaction rates of catalytic H_2O_2 decomposition, which will establish a steady-state concentration of H_2O_2 in the solution (as long as parameters such as water chemistry, flow rate, etc. remain constant). In previous work, H_2O_2 concentrations ranging from 10^{-6} to 10^{-3} mol/L were reported (*6*, *48*), so the values used here are in a realistic range. However, investigations in static systems cannot yield results on the mechanisms that govern the dynamic case. Under these aspects, it can be considered possible that, in a radiolytic repository system when Fe(II) and H_2O_2 are present in sufficient local concentrations, a radio-Fenton reaction might take place, similar to the photo-Fenton reaction observed for UV-irradiated systems (*15*, *39*, *49*, *50*). UO_2 could play the role of the inorganic acceptor in such a system. The reaction path of this specific case would depend strongly on factors such as water chemistry (e.g., presence of complexing groundwater ions or ionic radical scavengers), metallic surfaces (Fe(0) or noble metals), and precipitation of solid Fe(III) phases. For example, in a repository in contact with air [Fe(II)] would be much lower, and H_2O_2 might react preferentially with solid Fe(III) compounds (as investigated in ref *22*).

A perturbing factor in the development of "ideal" Fenton chemistry in groundwater systems is the ubiquitous presence of complexing anions (such as carbonate, phosphate, and others). It was shown that Fe(II) in the presence of such anions can react differently as compared to free Fe(II) and that, even in the presence of hydrogen peroxide, observation of the $^{\bullet}OH$ radical production can be obscured by the presence of other reactive species (*51*). The divergent effects of the tested representative anions cannot be explained as a correlation with the rate constants of the anions with $^{\bullet}OH$ (*19*). With regard to the stability constants of Fe(II) with the anions, a much better correlation exists (*52*). Nevertheless, the fast depletion of the DMPO−OH signal in the ESR/spin-trapping studies by carbonate may be a bonus, pointing to a decreased Fenton activity in carbonated groundwater.

Acknowledgments

The authors acknowledge Dr. M. Kelm and Prof. T. Fanghänel (INE Institute of Nuclear Waste Management) for model calculations with the code MAKSIMA-CHEMIST and for fruitful discussions; Drs. I. Ray, T. Wiss, and V. Rondinella and Mr. H. Thiele for help and advice on electron microscope techniques and facilities; Prof. J. Bruno for his helpful comments on the application of classical kinetics to waste management problems; and Prof. K. Lützenkirchen for support with analytical techniques.

Literature Cited

(1) Johnson, L.; Shoesmith, D. Spent fuel. In *Radioactive Waste Forms for the Future*; Lutze, W., Ewing, R., Eds.; Elsevier: Amsterdam, 1988.
(2) Silva, R.; Nitsche, H. Actinide environmental chemistry. *Radiochim. Acta.* **1995**, *70/71*, 377.
(3) Miller, W.; Alexander, R.; Chapman, N.; McKinley, I.; Smellie, J. *Geological Disposal of Radioactive Wastes & Natural Analogues*; Waste Management Series 2; Pergamon/Elsevier: Amsterdam, 2000.
(4) Burns, P., Finch, R., Eds. *Uranium*: *Mineralogy*, *Geochemistry and the Environment*; Reviews in Mineralogy 38; Mineralogical Society of America: Washington, DC, 1999.
(5) Shoesmith, D. J. Fuel corrosion processes under waste disposal conditions. *Nucl. Mater.* **2000**, *282*, 1.
(6) Christensen, H. Calculations simulating spent-fuel leaching experiments. *Nucl. Technol.* **1998**, *124*, 165.
(7) Kelm, M.; Bohnert, E. Radiolysis and corrosion of ^{238}Pu-doped UO_2 pellets in chloride brine. *Proc. Indian Acad. Sci.* (*Chem. Sci.*) **2002**, *114*, 697.
(8) Corbel, C.; Sattonay, G.; Lucchini, G.-F.; Ardois, C.; Barthe, M.-F.; Huet, F.; Dehaudt, P.; Hickel, B.; Jegou, C. Increase of the uranium release at an UO_2/H_2O interface under He^{2+} ion beam irradiation. *Nucl. Instrum. Methods Phys. Res. B* **2001**, *179*, 225.
(9) Schumb, W.; Satterfield, C.; Wentworth, R. *Hydrogen Peroxide*; American Chemical Society Monograph Series 128; Reinhold Publishing Corp./Chapman & Hall: New York/London, 1955.
(10) Amme, M. Contrary effects of the water radiolysis product H_2O_2 upon the dissolution of nuclear fuel in natural ground water and deionized water. *Radiochim. Acta* **2002**, *90*, 399.
(11) Loida, A.; Grambow, B.; Geckeis, H. Anoxic corrosion of various high burnup spent fuel samples. *J. Nucl. Mater.* **1996**, *238*, 11.
(12) Savoye, S.; Legrand, L.; Sagon, G.; Lecomte, S.; Chausse, A.; Mesina, R.; Toulhoat, P. Experimental investigations on iron corrosion products formed in bicarbonate/carbonate-containing solutions at 90 °C. *Corros. Sci.* **2001**, *43*, 2049.
(13) Barb, W. G.; Baxendale, J. H.; George, P.; Hargrave, K. R. Reactions of ferrous and ferric ions with H_2O_2. II. The ferric ion reaction. *Trans. Faraday Soc.* **1951**, *47*, 591.
(14) Voelker, B.; Sulzberger, B. Effects of fulvic acid on Fe(II) oxidation by hydrogen peroxide. *Environ. Sci. Technol.* **1996**, *30*, 1106.
(15) Zepp, R. G.; Faust, B. G.; Hoigné, J. Hydroxyl radical formation in aqueous reactions (pH 3−8) of iron(II) with hydrogen

peroxide: The photo-Fenton reaction. *Environ. Sci. Technol.* **1992**, *26*, 313.
(16) Bray, W. C.; Gorin, M. H. Ferryl ion, a compound of tetravalent iron. *J. Am. Chem. Soc.* **1932**, *54*, 2124.
(17) Jacobsen, F.; Holcman, J.; Sehested, K. Reactions of the ferryl ion with some compounds found in cloud water. *Int. J. Chem. Kinet.* **1998**, *30*, 215.
(18) Martire, D. O.; Caregnato, P.; Furlong, J.; Allegretti, P.; Gonzalez, M. C. Kinetic study of the reactions of oxoiron(IV) with aromatic substrates in aqueous solutions. *Int. J. Chem. Kinet.* **2002**, *34*, 488.
(19) Buxton, G. V.; Greenstock, C. L.; Helman, W. P.; Ross, A. B. Critical review of rate constants for reactions of hydrated electrons, hydrogen atoms and hydroxyl radicals ($^{\bullet}OH/O^{-}$) in aqueous solution. *J. Phys. Chem. Ref. Data* **1988**, *17*, 513.
(20) Sychev, A. Ya.; Isak, V. G. Iron compounds and the mechanisms of the homogeneous catalysis of the activation of O_2 and H_2O_2 and of the oxidation of organic substrates. *Russ. Chem. Rev.* **1995**, *64*, 1105.
(21) Tachiev, G.; Roth, J.; Bowers, R. Kinetics of hydrogen peroxide decomposition with complexed and 'free' iron catalysts. *Int. J. Chem. Kinet.* **2000**, *32*, 24.
(22) Kwan, W.; Voelker, B. Decomposition of hydrogen peroxide and organic compounds in the presence of dissolved iron and ferrrihydrite. *Environ. Sci. Technol.* **2002**, *36*, 1467.
(23) Rush, J. D.; Bielski, B. H. J. Pulse radiolysis studies of alkaline Fe(III) and Fe(IV) solutions. Observation of transient iron complexes with intermediate oxidation states. *J. Am. Chem. Soc.* **1986**, *108*, 523.
(24) Stuglik, Z.; Zagorski, Z. P. Pulse radiolysis of neutral iron(II) solutions: oxidation of ferrous ions by OH radicals. *Radiat. Phys. Chem.* **1981**, *17*, 229.
(25) Rush, J. D.; Bielski, B. H. J. Pulse radiolysis studies of the reactions of HO_2/O_2^- with Fe(II)Fe(III) ions. The reactivity of HO_2/O_2^- with ferric ions and its implications on the occurrence of the Haber−Weiss reactions. *J. Phys. Chem.* **1985**, *89*, 5062.
(26) Gallard, H.; De Laat, J.; Legube, B. Spectrophotometric study of the formation of iron(III)−hydroperoxy complexes in homogeneous aqueous solutions. *Water Res.* **1999**, *33*, 2929.
(27) De Laat, J.; Gallard, H. Catalytic decomposition of hydrogen peroxide by Fe(III) in homogeneous aqueous solution: Mechanism and kinetic modeling. *Environ. Sci. Technol.* **1999**, *33*, 2726.
(28) Baker, F.; Newton, T. The reaction between uranium(IV) and hydrogen peroxide. *J. Phys. Chem.* **1961**, *65*, 1897.
(29) Betts, R. Kinetics of the oxidation of uranium(IV) by iron(III) in aqueous solutions of perchloric acid. *Can. J. Chem.* **1955**, *33*, 1780.
(30) Haber, F.; Weiss, J. The catalytic decomposition of H_2O_2 by iron salts. *Proc. R. Soc., Ser. A* **1934**, *147*, 332.
(31) Gallard, H.; de Laat, J. Kinetic modelling of Fe(III)/H_2O_2 oxidation reactions in dilute aqueous solution using atrazine as a model compound. *Water Res.* **2000**, *34*, 3107.
(32) Chou, S.; Huang, C. Application of a supported iron oxyhydroxyde catalyst in oxidation of benzoic acid by hydrogen peroxide. *Chemosphere* **1999**, *38*, 2719.
(33) Halpern, J.; Smith, J. Kinetics of the oxidation of uranium(IV) by molecular oxygen in aqueous perchloric acid solution. *Can. J. Chem.* **1956**, *34*, 1419.
(34) Teply, J.; Stulik, V. Formation of peroxidic precipitate in the radiolysis of uranyl nitrate ketone solutions. *Nature* **1963**, *200*, 671.
(35) Hughes Kubatko, K.-A.; Helean, K.; Navrotsky, A.; Burns, P. Stability of peroxide-containing uranyl minerals. *Science* **2003**, *14*, 302, 1191.
(36) Bader, H.; Sturzenegger, V.; Hoigné, J. Photometric method for the determination of low concentrations of hydrogen peroxide by the peroxidase-catalysed oxidation of DPD. *Water Res.* **1988**, *22*, 1109.
(37) Stookey, L. Ferrozine—a new spectrophotometric reagent for iron. *Anal. Chem.* **1970**, *42*, 779−781.
(38) Saran, M.; Summer, K. H. Assaying for hydroxyl radicals: Hydroxylated terephthalate is a superior fluorescence marker than hydroxylated benzoate. *Free Radical Res.* **1999**, *31*, 429.
(39) Bossmann, S. H.; Oliveros, E.; Gäb, S.; Siegwart, S.; Dahlen, E. P.; Payawan, L.; Straub, M.; Wörner, M.; Braun, A. M. New evidence against hydroxyl radicals as reactive intermediates in the thermal and photochemically enhanced Fenton reactions. *J. Phys. Chem.* **1998**, *102A*, 5542.
(40) Hug, S.; Leupin, O. Iron-catalysed oxidation of arsenic(III) by oxygen and by hydrogen peroxide: pH-dependent formation of oxidants in the Fenton reaction. *Environ. Sci. Technol.* **2003**, *37*, 2734.
(41) Ensing, B.; Buda, F.; Baerends, E. J. Reaction path sampling of the reaction between iron(II) and hydrogen peroxide in aqueous solution. *J. Phys. Chem.* **2002**, *107A*, 5722.
(42) Kelm, M.; Bohnert, E. A kinetic model for the radiolysis of chloride brine. FZKA Report 6977; Forschungszentrum Karlsruhe Wissenschaftliche Berichte: Karlsruhe, 2004.
(43) Finkelstein, E.; Rosen, G. M.; Rauckman, E. J.; Paxton, J. Spin trapping of superoxide. *Mol. Pharmacol.* **1979**, *16*, 676.
(44) Grenthe, I. (Chairman), Wanner, H., Forest, I., Eds. *Chemical Thermodynamics Vol. 1—Chemical Thermodynamics of Uranium*; NEA-OECD; North-Holland: Amsterdam; 1992.
(45) De Pablo, J.; Casas, I.; Gimenez, J.; Molera, M.; Rovira, M.; Duro, L.; Bruno, J. The oxidative dissolution mechanism of uranium dioxide. I. The effect of temperature in hydrogen carbonate medium. *Geochim. Cosmochim. Acta* **1999**, *63*, 3097.
(46) Cui, D.; Spahiu, K. The reduction of U(VI) on corroded iron under anoxic conditions. *Radiochim. Acta* **2002**, *90*, 623.
(47) Celeda, J.; Gomez Lara, J. The kinetics and mechanism of the dissolution of uranous-uranic oxide in sulphuric acid in the presence of ferric iron. *J. Inorg. Nucl. Chem.* **1965**, *27*, 2561.
(48) Fattahi, M.; Houee-Levin, C.; Ferradini, C.; Jacquier, P. Hydrogen peroxide formation and decay in γ-irradiated clay water. *Radiat. Phys. Chem.* **1992**, *40* (3), 167.
(49) Pignatello, J. J.; Liu, D.; Huston, P. Evidence for an additional oxidant in the photoassisted Fenton reaction. *Environ. Sci. Technol.* **1999**, *33*, 1832.
(50) Kiwi, J.; Lopez, A.; Nadtochenko, V. Mechanism and kinetics of the OH-radical intervention during fenton oxidation in the presence of a significant amount of radical scavenger (Cl^-). *Environ. Sci. Technol.* **2000**, *34*, 2162.
(51) Saran, M.; Michel, C.; Stettmaier, K.; Bors, W. Arguments against the significance of the Fenton reaction contributing to signal pathways under in vivo conditions. *Free Radical Res.* **2000**, *33*, 567.
(52) King, D. W.; Farlow, R. Role of carbonate speciation on the oxidation of Fe(II) by H_2O_2. *Mar. Chem.* **2000**, *70*, 201.

Received for review March 8, 2004. Revised manuscript received September 27, 2004. Accepted October 1, 2004.

ES040034X